Construction and Building Materials 319 (2022) 126081

Contents lists available at ScienceDirect

Construction and Building Materials

journal homepage: www.elsevier.com/locate/conbuildmat

Influence of self-healing induced by polylactic-acid and alkanoates-derivates precursors on transport properties and chloride penetration resistance of sound and cracked mortar specimens

Emanuele Rossi [a,*], Rahul Roy [b], Oguzhan Copuroglu [a], Henk M. Jonkers [a]

[a] Delft University of Technology, Faculty of Civil Engineering & Geosciences - Department of Materials & Environment, Stevinweg 1, 2628 CN Delft, The Netherlands
[b] KU Leuven, Department of Materials Engineering (MTM), Kasteelpark Arenberg 44/bus 2450, 3001 Leuven, Belgium

ARTICLE INFO

Keywords:
Self-healing
Bacteria
Chloride penetration
Durability

ABSTRACT

The possible beneficial impact of self-healing on chloride transport through cracks has been assessed for two bacteria-based self-healing mortar mixtures in comparison with Ordinary Portland cement mortar. Intact self-healing specimens featured lower chloride transport coefficients thanks to a denser microstructure and to the formation of a layer of calcium carbonate on their surface. However, self-healing of cracks of cracked mortar specimens did not significantly reduce chloride penetration during 28 days of chloride exposure compared to cracked and non-healed specimens. On the other hand, this study demonstrated that self-healing of 150–200 μm wide cracks reduced chloride ingress during shorter term (14 days) chloride exposure in comparison to cracked but non-healed specimens. The results of this study suggest that self-healing of cracks through calcium carbonate formation results in water blockage (sealing) of cracks but that the limited amount of limestone formed creates an imperfect barrier against diffusion of chloride ions through the apparent porous limestone. The short-term positive effect of self-healing with respect to reduced chloride ingress could be beneficial in applications where chloride exposure is limited or non-permanent such as concrete structures irregularly exposed to deicing salts or located in the splash zone in marine environments.

1. Introduction

The durability of concrete is a major issue for both industry and academia worldwide. Because of the brittle nature and the low tensile strength of concrete, cracks are an unavoidable phenomenon affecting structures. Cracks allow harmful agents present in the environment to penetrate the material, reducing its service life and structural reliability and increasing its repair and maintenance costs. However, some cracks do not negatively influence the service life of structures since concrete has an intrinsic autogenous capacity to self-heal them [1]. This self-healing capacity (SHC) is dependent on many parameters, such as the type of cement and water to cement ratio (w/c) of the mixture, age of cracking and the crack width. Autogenous healing occurs through continuous hydration of cement particles and through precipitation of calcium carbonate resulting from carbonation of the matrix [2]. The capacity of concrete to self-heal cracks autogenously is generally limited to cracks up to 100–150 μm wide [3]. However, previous studies reported that the width of cracks that concrete could self-heal varied from 5 to 10 μm to 300 μm [4–9]. By healing a crack completely it is expected that less or no harmful agents from the outside environment (i.e. CO_2 and chlorides) can penetrate the material thus resulting in an increase of service life of the concrete structure. This assumption is confirmed by many studies that investigated the effectiveness of autogenous healing of micro-cracks in reducing the chloride penetration of concrete as a function of many inter-related parameters [4,10–14]. E.g. Jacobsen et al. [4] observed that three months self-healing of cracked concrete led to a reduction of around 30% of the chloride migration rate compared to that of freshly cracked specimens. Darquennes et al. [10] demonstrated the higher capacity of mixtures with added-in blast-furnace slag to limit chloride penetration in cracked concrete thanks to higher autogenous self-healing compared to more traditional mixtures (i.e. predominantly based on Portland cement). As a result, self-healed specimens could be considered as sound specimens characterized by small cracks. Sahmaran et al. [11] investigated the effectiveness of self-healing for chloride penetration of Engineered Cementitious Composites (ECCs) containing different supplementary cementitious materials (SCMs) exposed to

* Corresponding author.
E-mail address: e.rossi@tudelft.nl (E. Rossi).

https://doi.org/10.1016/j.conbuildmat.2021.126081
Received 8 July 2021; Received in revised form 2 December 2021; Accepted 9 December 2021
Available online 16 December 2021

different healing regimes for two months. Beside observing that the self-healing capacity of the mixture appeared highly dependent on the added-in SCM as well as on the healing regime to which the cracked specimens were exposed, Rapid Chloride permeability test (RCPT) showed that the duration of the healing regimes and the chlorides ingress in self-healed specimens appeared inversely proportional. In some cases, the chlorides ingress of self-healed specimens was four to ten times lower than that of freshly cracked specimens. Yoon and Schlangen [12] observed that complete self-healing of 25 μm wide cracks blocked chlorides ingress and, consequently, restored the chloride penetration resistance to that of un-cracked specimens. Furthermore, they reported that micro-cracks with a width equal or lower than 40 μm did not significantly influence the chloride penetration properties of cracked concrete. This finding is in agreement with the study of Ismail et al. [13], who reported that for crack openings smaller than 30 μm no chloride diffusion occurred along the crack path. Besides observing that the chloride diffusion rate decreased with decreasing crack width, they confirmed that self-healing of mortar specimens can impede chlorides diffusion in the matrix for cracks less than 60 μm wide. Similar results were obtained by Sahmaran [14], who tested the chloride diffusivity of mortar specimens with different crack width. In latter study, it was observed that chlorides transport along a crack path was significantly mitigated for crack widths less than 50 μm thanks to self-healing. Also, it was reported that crack widths smaller than 135 μm only show marginal effects on the effective diffusion coefficient of mortar specimens, while crack widths larger than 135 μm can seriously reduce the service life of concrete structures through acceleration of initiation of steel bar corrosion.

Thanks to the capacity to mitigate chlorides penetration in cracked specimens, self-healing of cracks can have a positive impact on concrete durability, hence increasing its service life and decreasing the costs of repair and maintenance of infrastructures. However, based on the results reported in the literature, this capacity is apparently limited to cracks up to around 50 μm wide, which is equal to half or up to one third of the crack width that concrete can self-heal autogenously (i.e. 100–150 μm) [3]. To what extend only partial healing of cracks (e.g. through crack-bridging on one or several locations along the crack depth or crack closure at the surface) only results in an improvement of chloride penetration resistance remains however as yet unclear. Theoretically, surface crack closure might block the penetration of chlorides. However, this block might be only temporary if the crack-filling material is porous and particularly when cracks do not completely self-heal over the full crack depth. So far, a lot of research has been conducted with the aim to increase the self-healing of concrete beyond its autogenous capacity, by means of adding different types of healing agents to the concrete mix. Among others, the most studied healing agents that have been proposed are Superabsorbent Polymers (SAPs), dispersed organic polymers (i.e. epoxy resin), macro- and micro-encapsulated polymers or (expansive) minerals (i.e. microfluidics or glass capsules) and bacteria-based agents that can be dispersed in the matrix, encapsulated (i.e. in hydrogels or polymeric substrates) or impregnated in carriers (i.e. porous granules) [3]. Higher autonomous self-healing capacity allows the material to heal wider cracks as well as to heal cracks with a given width in a shorter time than through autogenous healing only. The self-healing performance of these engineered technologies has been generally assessed and reported in literature through, among other methods, microscopic observations of the crack closure over time, regain of water tightness and regain of structural capacity [15]. Even though the higher self-healing capacity of these technologies has been demonstrated, the positive influence that improved self-healing might have on reduction of chloride penetration has been only scarcely reported [16]. Van Mullen et al. [16] investigated the influence of SAPs on chloride ingress in both un-cracked concrete and concrete featuring 107–153 μm wide cracks. As a result, SAPs had marginal positive influence since the chloride penetration depth for specimens previously cracked and subsequently healed for five weeks was similar for both plain (reference) and SAPs-containing mortar. Furthermore, it was pointed out that un-cracked specimens containing SAPs had lower chloride penetration resistance than plain mortar specimens. This fact was related to the higher content of water that must be added in SAPs-containing mixtures to compensate their loss in workability due to SAPs absorption, hence increasing the porosity of the mixture. Wang et al. [17] investigated the influence of self-healing promoted by organic healing agents (urea formaldehyde encapsulated epoxy) to mitigate chloride penetration. Specimens with different amounts of healing agents (0%, 3% and 6%) were pre-loaded up to 50% of their maximum compression strength. Even though no induced crack characterization was provided, the addition of micro-capsules significantly improved the chloride penetration resistance of healed specimens. For specimens containing 6% of microcapsules, the chloride diffusion coefficient of healed specimens was equal to that of un-cracked specimens. Maes et al. [18] studied the effectiveness of polyurethane based healing agents to improve the chloride resistance of cracked specimens (100–300 um). The healing agent was applied either manually on the surface of the specimens or added encapsulated to the mix during casting. After manual repair, 83% and 67% of the specimens with crack widths of 100 μm and 300 μm, respectively, showed almost no chloride penetration around the healed crack. For encapsulated healing agents, the influence on chloride diffusion resistance was less beneficial but still substantial. Further work on encapsulated polyurethane based agents was conducted by Van Belleghem et al. [19]. In their study, the negative influence of 300 μm wide cracks on chloride resistance was shown both in terms of chloride penetration depth and matrix chloride concentration. In cracked specimens containing polyurethane healing agents, a reduction of chloride concentration of around 75% was observed around the crack thanks to self-healing, even though it was reported that complete healing of the crack was not achieved.

In order to achieve higher chloride resistance of cracked concrete structures through increased self-healing, expectedly resulting in increased service life performance, a significant reduction of chloride ingress through healed cracks in comparison to unhealed cracks must occur. Therefore, in this study the effectiveness of self-healing to mitigate chloride penetration in cracked mortar specimens has been assessed for two mixtures containing different bacteria-based healing agents (i.e. one poly-lactic acid- and one alkanoate-based healing agent) in comparison to reference (no healing agent containing) mortar specimens. The improvement of self-healing capacity of mortar specimens with respect to restoring water tightness of cracks up to 500 μm wide has been previously reported for both types of these bacteria-based healing agents [20–21]. Latter studies showed the high potential for applying both the healing agents in practice as negligible influence of the poly-lactic acid (PLA)- and alkanoates-derivates (AKD) based particles on other concrete functional properties was demonstrated. However, the possible beneficial influence that self-healing of cracks might have on reduction of chloride penetration for both the bacteria-based mixtures had not been assessed yet. Some previous studies showed that self-healing of cracks did not significantly improve chloride penetration resistance even though cracks were partially or completely healed [16,18]. Hence, the potential to restore chloride penetration resistance for cracked specimens with and without added PLA and AKD particles is therefore addressed in the present study.

This paper presents an experimental investigation on chloride penetration resistance of bacteria-based self-healing mortar specimens. The chloride migration and diffusion coefficients were assessed for both cracked and un-cracked specimens made of self-healing mortars and compared to those of plain (reference) mortar. The effectiveness of self-healing to mitigate chlorides penetration in cracked mortar has been also evaluated for the different mixtures. The main objective of this research was to assess the influence that PLA and AKD healing agents have on chloride penetration resistance of sound (un-cracked) and cracked specimens in comparison to reference mortar specimens. Results can be used to predict service life performance of structures made with or without added bacteria-based healing agent.

2. Materials and methods

2.1. Healing agents

Alkanoate-derived healing agent (AKD) particles were composed of alkanoate, bacterial spores of *Bacillus cohnii*-related strains and growth-required nutrients (i.e., yeast extract). Alkanoate-rich biomass was obtained from a pilot plant that uses the organic fraction of municipal waste (OFMSW) as raw material (Orgaworld/Paques, Lelystad, Netherlands). Alkanoate was extracted from the biomass with a solvent-based method under laboratory conditions. Healing agent particles were obtained by merging alkanoate, bacterial spores and growth requiring nutrients (i.e., yeast extract) through compaction. More information about the formulation of AKD particles can be found elsewhere [20]. PLA-based healing agent obtained from Basilisk B.V. (Delft, Netherlands) was composed of lactate derivatives, bacterial spores of *Bacillus cohnii*-related strains and nutrients. Both the healing agent particles had a particle size of 0.5–1 mm.

2.2. Mortar mixtures

Three mortar mixtures with and without added-in healing agents were cast to investigate their chloride penetration resistance. Each mortar mixture was composed of Ordinary Portland cement (OPC, CEM I 42.5 N, ENCI, Rotterdam, Netherlands) and fine siliceous aggregates in a proportion of 1:3. The aggregates maximum size (D_{max}) was 2 mm and the water-cement ratio (w/c) was equal to 0.5 for all mixtures. One plain mortar mixture (reference) was cast with no healing agent addition (labelled as Ctrl). Two further self-healing mortar mixtures were cast with added-in 2.6% w/w_{cement} of either PLA or AKD healing agents, labelled as PLA and AKD mixtures, respectively. The composition of each mortar mixture is reported in Table 1.

For all the specimen configurations used to evaluate the chloride penetration resistance tests reported later, each mortar mixture was cast according to the following procedure. All dry components were mixed for 1 min at low speed through a Hobart planetary mixer. Water was added into the running mixer in the following 30 s and the components were left to mix for extra 30 s. Afterwards, the walls of the mixer were scraped and mixing was continued for 1 min and 30 s at low speed and 30 s at medium speed. The properties of hardened mortars are reported in Table 2.

2.3. Chloride penetration resistance tests

2.3.1. Chloride diffusion in sound specimens

The chloride diffusion test in sound specimens was carried out in accordance with standard NT Build 443 [22]. The test was conducted on 40 × 40 × 40 mm^3 cubic specimens obtained from 40 × 40 × 160 mm^3 prism moulds. After casting, the prismatic specimens were sealed with plastic sheet and left to harden for 24 h at laboratory conditions (T = 20 °C and RH = 80 %). Afterwards the specimens were demoulded and stored in a fog chamber with temperature and relative humidity set at 20 °C and 95 %, respectively, until the age of 28 days. At 28 days of age the specimens were sawn in 40 × 40 × 40 mm^3 cubes and the lateral cube faces were sealed with waterproof tape and epoxy resin. The specimens were completely immersed in a 10% concentrated sodium chloride (NaCl) solution for 60 days in airtight plastic containers. Sample containers were shaken once a week. After five weeks of exposure, the liquid was replaced with a fresh solution. At the end of 60 days, the samples were removed from the solution. For each mortar mixture, one specimen was split for the determination of the chloride penetration depth by spraying a 0.1 M silver nitrate ($AgNO_3$) solution. The chloride penetration (concentration) profiles were measured in the three remaining specimens immediately after the exposure period, by grinding off distinct material layers and determining their total chloride content according to RILEM TC 178-TMC [23]. The chloride diffusion coefficient was obtained by fitting the measured concentration profile to the 2nd Fick's law expressed as Eq. (1).

$$C(x,t) = C_s - (C_s - C_i)\mathrm{erf}(x/\sqrt{4D_e t}) \quad (1)$$

where C(x, t) is the chloride concentration measured at the depth ×, at an exposure time t in mass %. C_S is the chloride concentration at the surface expressed in mass %. C_i is the initial chloride concentration of the mortar mixture expressed in mass % and D_e is the effective chloride transport coefficient in m^2/s.

2.3.2. Chloride migration in sound specimens

The non-steady state chloride migration coefficient of each mixture was measured through the Rapid Chloride Migration (RCM) test. For each mixture, two cylindrical specimens with 50 mm height and 100 mm diameter were sawn from 200 mm-high mortar cylindrical specimens. Specimens' preparation, pre-conditioning and test conduction were carried out in accordance with standard NT Build 492 [24] at laboratory conditions (T = 20 °C and RH = 80 %). With the voltage preset at 30 V, the resulting initial current (I_0) was between 90 and 120 mA for all the specimens. Following the indications given in NT Build 492, the applied voltage (U) to conduct the test was equal to 20 V and the test duration was 24 h. When the test was completed, the samples were disassembled from the experimental set-up and dried with a cloth. Afterwards, each specimen was split perpendicularly to the crack and the chloride penetration was determined through colour change after spraying the halves of the specimen with 0.1 M $AgNO_3$ solution. Images of the sprayed surface were collected and later image analysis (i.e. measuring the average chloride penetration depth) was conducted through ImageJ. The lateral portions of the specimens (e.g. up to 10 mm far from the edges of the cross-section) were not considered in the measurements to avoid any side-effect from lateral chloride penetration. The average chloride penetration depth (x_d) was used to calculate the non-steady state migration coefficient according to Eq. (3):

$$D_{nssm} = \frac{0.0239(273+T)L}{(U-2)t}\left(x_d - 0.0238\sqrt{\frac{(273+T)Lx_d}{U-2}}\right) \quad (3)$$

Where D_{nssm} is the non-steady state migration coefficient ($x10^{-12}$ m^2/s), L is the thickness of the specimen (mm), U is the absolute value of applied voltage (U), t is the test duration (hours) and x_d is the average value of the penetration depths.

2.3.3. Chloride diffusion in cracked specimens

For each mortar mixture, four cylindrical specimens of 100 mm diameter were tested for chloride diffusion resistance in cracked samples. The fresh mixtures were poured in two cylindrical plastic moulds of

Table 1
Composition of mortar mixtures analysed in the present study.

Mixture	Cement type	w/c	Cement: aggregates	D_{max} (mm)	HA (% by mass of cement)
Ctrl	CEM I 42.5 N	0.5	1:3	2	0
PLA	CEM I 42.5 N	0.5	1:3	2	2.6
AKD/ PHBV	CEM I 42.5 N	0.5	1:3	2	2.6

Table 2
Properties of hardened mortar mixtures analysed in the present study (average of three replicates).

Mixture	Compression strength at 28 days (MPa)	Flexural strength at 28 days (MPa)
Ctrl	29.9 ± 1.6	1.7 ± 0.1
PLA	41.3 ± 4.9	1.9 ± 0.0
AKD	36.6 ± 3.4	1.7 ± 0.1

200 mm height, sealed with plastic sheet and left hardening for 24 h at laboratory conditions. Afterwards the specimens were demoulded and stored in a fog chamber with temperature and relative humidity set at 20 °C and 95 %, respectively, until the age of 28 days. At 28 days of age, the top, middle and bottom portion of the 200 mm-high specimens were sawn off to obtain two 75 mm-high cylindrical samples, for a total of four specimens for each mortar mixture. A notch of 5 mm × 5 mm was created on the top face of each cylinder through sawing. Afterwards, two stainless steel plates of 100 mm × 100 mm were glued on the top of the specimens to induce tensile forces and consequent crack formation. Linear Variable Displacement Transducers (LVDTs) holders were also glued on the sides of the specimens (two for each side) perpendicular to the loading direction, as schematically represented in Fig. 1.

When the glue was hardened, the steel plates glued at the top of the specimens were vertically attached to an Instron 8872 loading device, as schematically represented in Fig. 2. Prior to start each test, two LVDTs were calibrated and fixed on each side of the specimens to their respective holders to monitor the Crack Mouth Opening Displacement (CMOD). The tests were performed in deformation control mode up to a target CMOD of 250 μm, with a deformation rate equal to 0.2 μm/s. Each test was finished when the average displacement of the two LVDTs reached the target CMOD. After sample relaxation, the effective CMOD ($CMOD_{eff}$) was evaluated with optical microscopy analysis. Time, load, target and effective CMOD were continuously reported during the test, resulting in a load–displacement curve of which an example is shown in Fig. 2.

After crack induction, the top 5 mm of each sample were dry-sawn to obtain a flat surface, and optical microscope images of the surface cracks were collected. The lateral and bottom faces of each specimens were sealed with waterproof tape and epoxy resin to avoid any lateral penetration of chlorides. Afterwards, the four specimens of each mixture were placed in the following four different exposure conditions before chlorides profiling. Two specimens were submerged in 10% NaCl concentrated solution for 14 and 28 days at laboratory conditions, labelled as "Mixture_CDT_Cl14" and "Mixture_CDT_Cl28", respectively. The two remaining specimens were first left self-healing submerged in water at laboratory conditions for 28 days and then submerged in 10% NaCl concentrated solution for 14 and 28 days, labelled as "Mixture_CDT_SHCl14" and "Mixture_CDT_SHCl28", respectively. The latter specimens were used to evaluate the potential positive effect that self-healing has on chlorides penetration in cracked mortar. After the different exposures, optical microscope images of the surface cracks were collected and compared to the initial crack images to evaluate the degree of self-healing. The self-healing capacity (SHC) of each specimen was determined according to Eq. (2):

$$SHC = \frac{w_{eff,i} - w_{eff,t}}{w_{eff,i}} * 100$$

Where SHC is the self-healing capacity (%), $w_{eff,i}$ is the initial effective crack width (μm) and $w_{eff,t}$ is the effective crack width after exposure. Both the effective crack widths were determined as the average of 20 crack width measurements taken at intervals of 500 μm along the crack length. Afterwards, each specimen was split perpendicularly to the crack and the chloride penetration was determined through colour change after spraying the halves of the specimen with 0.1 M $AgNO_3$ solution. Images of the sprayed surface were collected and later image analysis (i.e. maximum chlorides penetration depth) was conducted through ImageJ.

2.3.4. Chloride migration in cracked specimens

Beside the determination of the non-steady state migration coefficient of sound specimens, the RCM test was also conducted to test the positive effect of self-healing on chloride penetration. For each mixture, six cylindrical specimens with 75 mm height and 100 mm diameter were obtained from 200 mm-high specimens as described in Section 2.3.3. The crack induction procedure was the same of that followed for the specimens tested for chloride diffusion resistance reported in Figs. 1-2. After surface crack image collection, the chloride penetration in three specimens was measured through the RCM test [24], as previously described in Section 2.3.2. These specimens were labelled as "Mixture_RCM_1-3". The remaining three specimens of each mixture were left self-healing submerged in water at laboratory conditions for 28 days, after which the RCM test was conducted. These specimens were labelled as "Mixture_RCM_SH_1-3". After each RCM test, the chloride penetration depth was measured according to the procedure described in Section 2.3.3.

2.4. Micro-Structural analysis

2.4.1. Scanning Electron microscope (SEM) analysis

After determining the chloride profiles of the cracked mortars, electron microscopy analysis was conducted on the specimens previously tested for chloride diffusion resistance (Section 2.3.2) to observe any possibly formed self-healing product precipitates at the crack mouth and along the crack depth. One half of each sample was vacuum impregnated with low viscosity fluorescent epoxy and sawn parallel to the splitting surface, to obtain a section perpendicular to the crack depth. Each section was then manually ground with #120, #220, #320, #600, #800 and #1200 silicon carbide sanding paper and polished with 6, 3, 1 and 0.25 μm polishing diamond paste on a lapping table to obtain a mirror-like surface. Each grinding and polishing step took around 10 min. Ethanol and non-water based polishing paste were used for grinding and polishing, respectively. Once polished, sections were coated with thin layer of gold (10 nm) to ensure surface conductivity. Scanning Electron Microscopy (SEM) with a Back Scattered Electrons (BSE) detector was performed on the sections to observe any formation of self-healing crystals along the crack depth. For this analysis, an Environmental Scanning Electron Microscope (ESEM, FEI, Quanta FEG 650, Thermo Fisher Scientific) was used at high vacuum for the acquisition of the micrographs. The micrographs were acquired at a voltage of

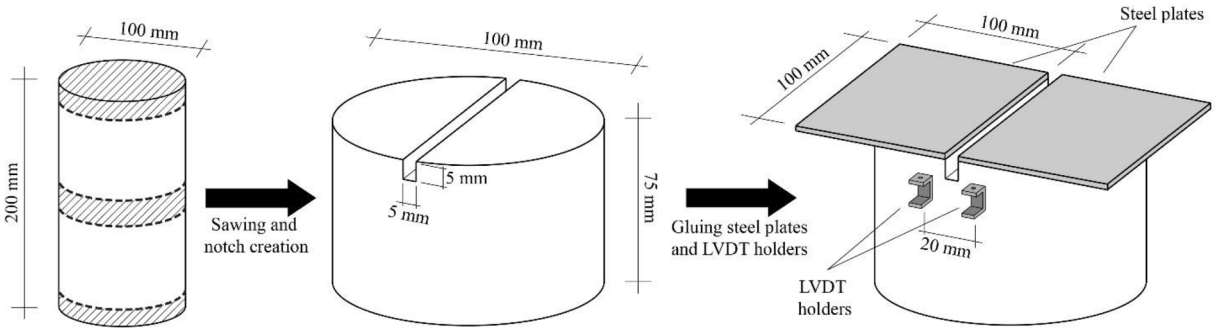

Fig. 1. Schematic representation of sample preparation before crack induction. (left) initial 200 mm-high cylindrical specimen (highlighting the removed portions); (centre) individual specimen layout after notch creation; (right) specimen layout after gluing steel plates and LVDT holders.

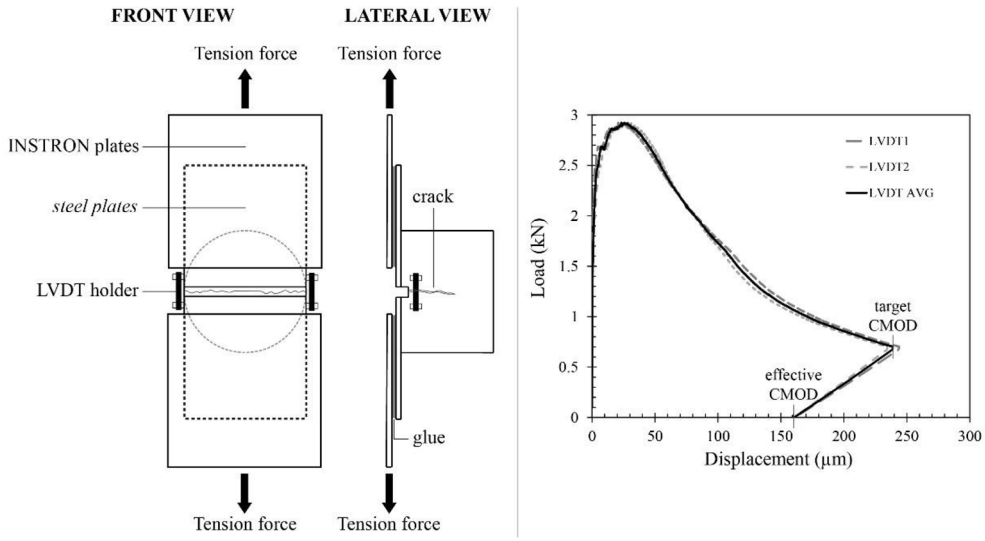

Fig. 2. Schematic representation of crack induction procedure. (left) front and lateral views of crack induction set-up; (right) example of load–displacement curve monitored to reach the target CMOD.

15 kV and with a magnification of 100x and 500x. A schematic representation of the whole experimental procedure is shown in Fig. 3.

2.4.2. Mercury intrusion Porosimetry (MIP) and thin sections

The pore size distribution and pore volume of specimens derived from each mixture was measured through Mercury Instrusion Porosimetry (MIP). For each mixture, one cylindrical specimen with 200 mm height and 100 mm diameter was cast, demoulded after 24 h and left curing in a high-humidity chamber (T = 20 °C and RH = 95 %) for 28 days. After curing, one cylindrical specimen with 50 mm height and 100 mm diameter was sawn from the initial cylindrical specimen and kept submerged in water for 28 days at laboratory conditions. After 28 days of water submersion each specimen was vertically sawn in two halves. The top portion (around 20 mm) of one half of each specimen was manually fragmented with a chisel and left drying in a vacuum freezer for pore water removal until no mass loss was anymore measurable (i.e. around 10 days). Then, the pore size distribution and pore volume of around 8 g of fragments of each mixture were determined through MIP using a Micromeritics AutoPore IV Mercury Porosimeter (Micromeritics Instruments Corporation). The other half of each specimen was vacuum impregnated with fluorescent epoxy and thin sections of the top portion the specimens were obtained according to the procedure reported by Jakobsen and Brown [25]. A schematic representation of this experimental procedure is reported in Fig. 4.

3. Results

3.1. Chloride diffusion and migration in sound specimens

The results of the chloride transport properties in sound specimens of each mixture are reported below. Fig. 5 shows the chloride profiles through which the chloride diffusion coefficients were determined according to NT Build 443 [22], while Table 3 reports a summary of the results obtained from both NT Build 443 and NT Build 492 [22,24].

From Fig. 5 and Table 3, it is visible that the chloride transport resistance of both PLA and AKD mixtures increased compared to that of the Ctrl mixture. The average chloride diffusion coefficients for Ctrl, PLA and AKD mixtures measured according to NT Build 443 are $11.6x10^{-12}$ m^2/s, $6.9x10^{-12}$ m^2/s and $8.4x10^{-12}$ m^2/s, respectively. The same trend is visible for data obtained according to the NT Build 492 procedure. The average chloride penetration depth for Ctrl, PLA and AKD were 25.4 mm, 22.5 mm and 22.8 mm, respectively, resulting in average chloride migration coefficients equal to $21.3x10^{-12}$ m^2/s, $18.8x10^{-12}$ m^2/s and $19.0x10^{-12}$ m^2/s, respectively.

3.2. Chloride diffusion in cracked specimens

The chloride diffusion resistance in cracked specimens was evaluated according to the procedure described in Section 2.3.3. The results of

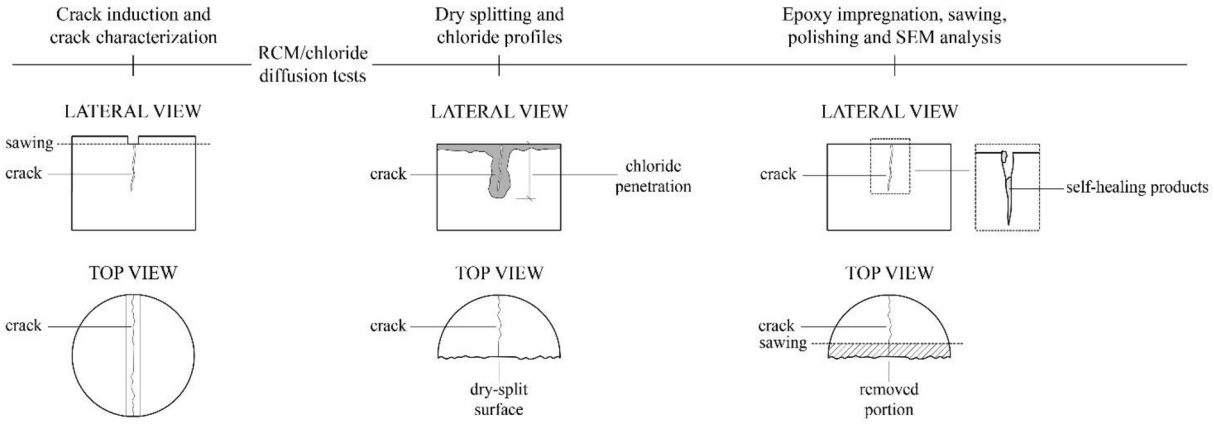

Fig. 3. Schematic representation of the sample preparation procedures applied for micro-structural analyses. (left) initial specimen layout; (centre) specimen after RCM/chloride diffusion test; (right) specimen subjected to SEM analysis.

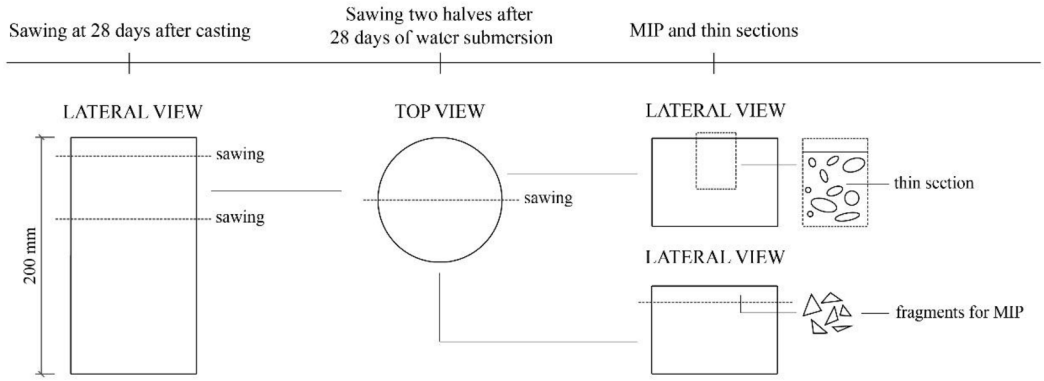

Fig. 4. Schematic representation of the sample preparation procedure from MIP and thin section analyses. (left) initial specimen layout after casting; (centre) top view of the specimen sawn in two halves; (right) specimens halves tested with MIP and from which thin sections were obtained.

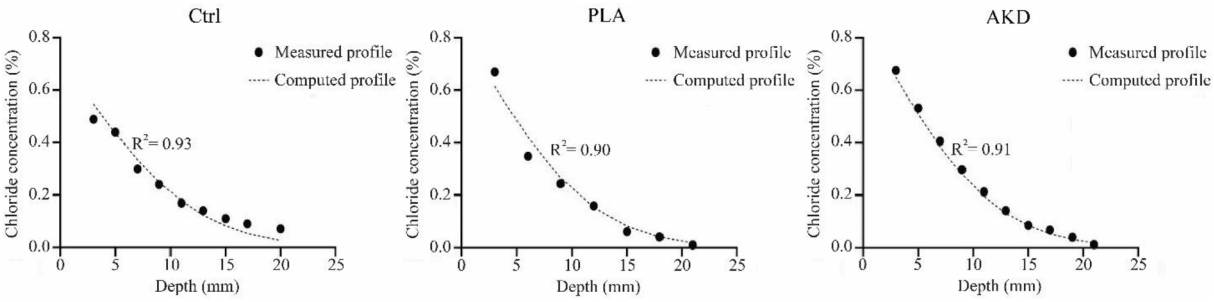

Fig. 5. Chloride concentration measured according to the procedure reported in NT Build 443 [22] for Ctrl, PLA and AKD specimens after 60 days of submersion in NaCl solution.

Table 3
Chloride diffusion and migration coefficients of sound (non-cracked) specimens determined according to NT Build 443 and NT Build 492.

Mixture	NT Build 443 Average chloride diffusion coefficient ($x10^{-12}$ m^2/s)	NT Build 492 Average chloride migration coefficient ($x10^{-12}$ m^2/s)	Average chloride penetration depth (mm)
Ctrl	11.6	21.3	25.4
PLA	6.9	18.8	22.5
AKD	8.4	19.0	22.8

each experimental phase for each specimen are reported in Table 4, namely the effective CMOD according to the Instron outputs ($CMOD_{eff}$), the effective crack width after microscopy analysis ($w_{eff,i}$), the self-healing capacity measured through microscopy analysis before measuring the chloride penetration profile (i.e. after each exposure) and the maximum chloride penetration after splitting. Microscopy images of the chloride profiles and surface cracks before and after each exposure for each specimen are shown in Figs. 6-7.

From the results shown in Table 4 and Figs. 6-7, it can be seen that the chloride penetration depth of cracked Ctrl, PLA and AKD specimens submerged for 14 days in NaCl solution ("Mixture_CDT_Cl14") were equal to 42.0 mm, 35.0 mm and 34.0 mm, respectively. Deeper chloride penetration was measured for all the specimens exposed to 28 days of NaCl solution ("Mixture_CDT_Cl28"), and these equalled to 44.5 mm, 44.5 mm and 47 mm, respectively. Surface crack images before and after self-healing show that complete self-healing occurred for all the specimens after 28 days of water submersion (Figs. 6-7). As a consequence, the chloride penetration depth decreased in all the specimens. The chloride penetration depth for Ctrl, PLA and AKD specimens exposed to 14 days of NaCl solution after self-healing ("Mixture_CDT_SHCl14") were equal to 24.5 mm, 19.5 mm and 22.0 mm, respectively, while that of the specimens exposed to 28 days of NaCl solution after self-healing ("Mixture_CDT_SHCl28") were equal to 41.5 mm, 38.0 mm and 36.0 mm, respectively.

Table 4
Characterization of cracked and self-healed specimens tested for chloride diffusion resistance (H_2O = water submersion; SH = self-healing; NaCl = submersion in 10% NaCl solution).

Specimen	$CMOD_{eff}$ (μm)	$w_{eff,i}$ (μm)	Exposure (days)	Self-healing capacity (%)	Chloride penetration depth (mm)
Ctrl_CDT_Cl14	174	162	14d NaCl	100	42
Ctrl_CDT_Cl28	177	164	28d NaCl	100	44.5
Ctrl_CDT_SHCl14	183	184	28d H_2O (SH) + 14d NaCl	100	24
Ctrl_CDT_SHCl28	177	173	28d H_2O (SH) + 28d NaCl	100	41.5
PLA_CDT_Cl14	158	172	14d NaCl	100	35
PLA_CDT_Cl28	157	155	28d NaCl	100	44.5
PLA_CDT_SHCl14	159	152	28d H_2O (SH) + 14d NaCl	100	19.5
PLA_CDT_SHCl28	147	168	28d H_2O (SH) + 28d NaCl	100	38
AKD_CDT_Cl14	166	172	14d NaCl	100	34
AKD_CDT_Cl28	191	178	28d NaCl	100	47
AKD_CDT_SHCl14	175	178	28d H_2O (SH) + 14d NaCl	100	22
AKD_CDT_SHCl28	162	152	28d H_2O (SH) + 28d NaCl	100	36

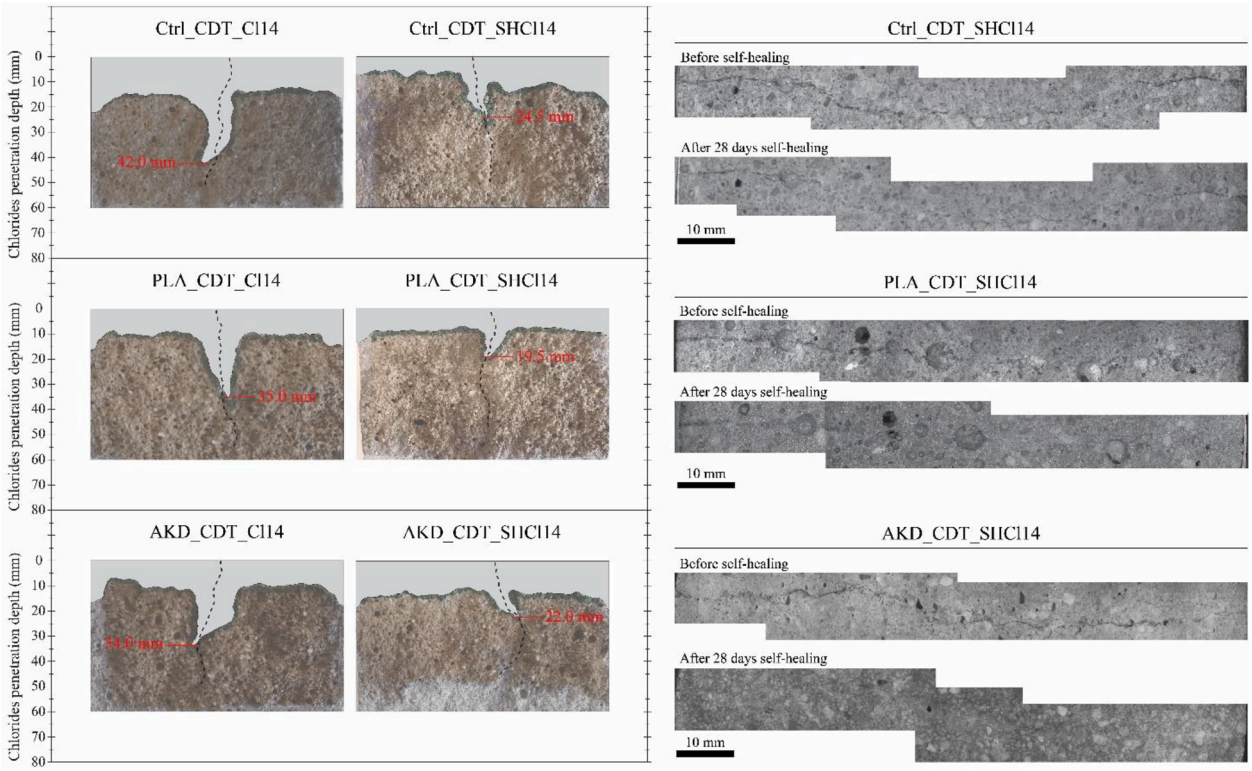

Fig. 6. Light microscope images of the specimens with and without self-healing submerged for 14 days in NaCl solution. (left) the dotted lines show the location of the original crack and the grey are represents the area of chloride ingress in the specimens while the value shown in red represents the maximum chloride penetration depth ("Mixture_CDT_Cl14" with no prior self-healing, "Mixture_CDT_SHCl14" with prior 28 days of self-healing); (right) surface crack images of the self-healed specimens before and after self-healing exposure (water submersion at laboratory conditions for 28 days). (For interpretation of the references to colour in this figure legend, the reader is referred to the web version of this article.)

3.3. Chloride migration in cracked specimens

The chloride migration resistance in cracked specimens was evaluated according to the procedure described in Section 2.3.4. The results are reported in Table 5, showing the effective CMOD according to the Instron outputs ($CMOD_{eff}$), the effective crack width after microscopy analysis ($w_{eff,i}$), the self-healing capacity measured through microscopy analysis and the maximum chloride penetration. Microscopy images of chloride penetration and appearance of surface cracks before and after each exposure for two specimens for each mixture are shown in Fig. 8.

From Table 5 and Fig. 8, it can be seen that the cracks of all the specimens exposed to water submersion for 28 days (i.e. "Mixture_RCM_SH_1-3") were completely self-healed. These cracks were ranging from a minimum width of 162 um to a maximum width of 198 um. However, complete self-healing of surface cracks did not noticeably improve the chloride penetration resistance compared to that of non-self-healed specimens. According to the results reported in Table 5, the average chloride penetration depth for Ctrl cracked specimens was equal to 37.2 mm, while that of Ctrl self-healed specimens even slightly increased up to 38.2 mm. A minimal decrease in chloride penetration was observed for both PLA and AKD specimens, reducing from 42.5 for cracked to 41.0 mm for self-healed PLA specimens and from 44.3 for cracked to 43.8 mm for self-healed AKD specimens.

3.4. SEM analysis of self-healing products in the crack depth

ESEM micrographs of specimens tested for chloride migration resistance are reported in Figs. 9-14.

From the SEM micrographs of specimens self-healed for either 14 days (Figs. 9-11) or 28 days (Figs. 12-14), it can be seen that several (multiple or branched) cracks instead of single ones were induced by the cracking procedure described in Section 2.3.3. Each specimen had overall one main crack of around 100–150 μm width, with several micro-cracks of around 30–50 μm width in its proximity. The micro-crack mouth of the self-healed specimens submerged for 14 days in NaCl solution appeared healed by a surface layer of precipitates with a thickness of around 50 μm (Fig. 9C–11C). On the other hand, the wider cracks were only partially self-healed (Fig. 9B-11B). Partial self-healing was clearly visible for Ctrl_CDT_SHCl14 and PLA_CDT_SHCl14 (Fig. 9B-10B), where the presence of crystals at the crack sides apparently did not fill or bridge the crack completely. Crack-bridging precipitates can be observed for AKD_CDT_SHCl14, but only as a layer with a few μm thickness (Fig. 11B). Deeper in the crack, self-healing for all the specimens exposed to 14 days of NaCl solution submersion was very limited. More effective self-healing could be observed for specimens submerged in NaCl solution for 28 days (Figs. 12-14). At the top of the crack mouth of Ctrl_CDT_SHCl28 a thin layer (e.g. a few μm thick) apparently bridging the crack top was present (Fig. 12A). For both PLA_CDT_SHCl28 and AKD_CDT_SHCl28, this healing layer was clearly thicker and denser, bridging the crack walls of both the specimens completely. Deeper in the cracks (e.g. at around 40 mm depth), bridging due to formation of self-healing precipitates could be partially or completely observed only at specific and limited locations, leaving the cracks mainly un-healed in all three mixtures (Fig. 12B-14B).

3.5. MIP results

The pore volume and the pore size distribution of specimens of each mixture according to MIP test are reported in Fig. 15.

According to the MIP test, PLA showed the lowest pore volume, equal to 0.054147 mL/g. Higher pore volume was measured for AKD, equal to 0.064405 mL/g, which was still slightly lower than the pore volume of

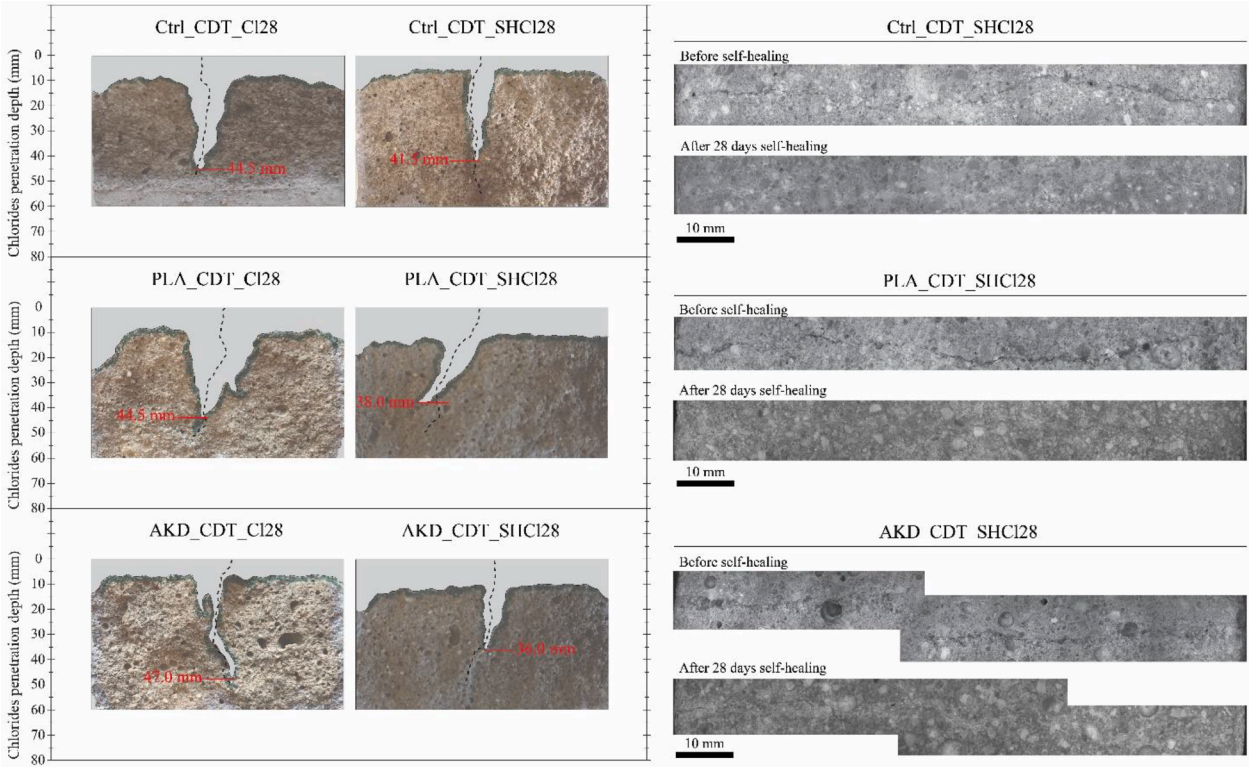

Fig. 7. Light microscope images of the specimens with and without self-healing submerged for 28 days in NaCl solution. (left) the dotted lines show the location of the original crack and the grey are represents the area of chloride ingress in the specimens while the value shown in red represents the maximum chloride penetration depth ("Mixture_CDT_Cl28" with no prior self-healing, "Mixture_CDT_SHCl28" with prior 28 days of self-healing); (right) surface crack images of the self-healed specimens before and after self-healing exposure (water submersion at laboratory conditions for 28 days). (For interpretation of the references to colour in this figure legend, the reader is referred to the web version of this article.)

Table 5
Characterization of cracked and self-healed specimens tested for chloride migration resistance (H_2O = water submersion; SH = self-healing).

Specimen	$CMOD_{eff}$ (μm)	$w_{eff,i}$ (μm)	Exposure (days)	Self-healing capacity (%)	Chloride penetration depth (mm)	Average penetration depth (mm)
Ctrl_RCM_1	166	184	RCM after cracking	–	40	37.2
Ctrl_RCM_2	161	180	RCM after cracking	–	34.5	
Ctrl_RCM_3	184	176	RCM after cracking	–	37	
Ctrl_RCM_SH_1	163	175	28d H_2O (SH)	100	41.5	38.2
Ctrl_RCM_SH_2	149	162	28d H_2O (SH)	100	37.5	
Ctrl_RCM_SH_3	193	198	28d H_2O (SH)	100	35.5	
PLA_RCM_1	169	168	RCM after cracking	–	46	42.5
PLA_RCM_2	193	172	RCM after cracking	–	37	
PLA_RCM_3	178	184	RCM after cracking	–	44.5	
PLA_RCM_SH_1	179	174	28d H_2O (SH)	100	44	41.0
PLA_RCM_SH_2	188	196	28d H_2O (SH)	100	39	
PLA_RCM_SH_3	178	180	28d H_2O (SH)	100	40	
AKD_RCM_1	191	186	RCM after cracking	–	40	44.3
AKD_RCM_2	215	200	RCM after cracking	–	46	
AKD_RCM_3	210	205	RCM after cracking	–	47	
AKD_RCM_SH_1	176	184	28d H_2O (SH)	100	41	43.8
AKD_RCM_SH_2	178	178	28d H_2O (SH)	100	44	
AKD_RCM_SH_3	192	186	28d H_2O (SH)	100	46.5	

the Ctrl specimen, equal to 0.066744 mL/g. Two major pore size classes could be observed for the Ctrl specimen (i.e. 0.01–0.1 μm and 1–10 μm). A significant presence of 1–10 μm pores was also present in the PLA matrix, while AKD mixture showed the highest presence of smaller pores, ranging between 0.01 and 0.1 μm.

4. Discussion

4.1. Transport properties of sound specimens

In this study, the chloride diffusion coefficients of sound (non-cracked) mortar specimens made from different mix designs were determined measured according to the NT Build 443 (free chloride diffusion) and NT Build 492 (Rapid Chloride Migration) procedures. Comparison between these two methods show that obtained chloride diffusion coefficients differ markedly (Fig. 16). The chloride diffusion coefficients determined according to the free diffusion test appeared in fact were two to three times smaller than those obtained via the Rapid Chloride Migration procedure.

The agreements between chloride migration and diffusion tests in sound mortar depends on the both the material quality in addition to the calculation method [26]. Even though it could be assumed that natural

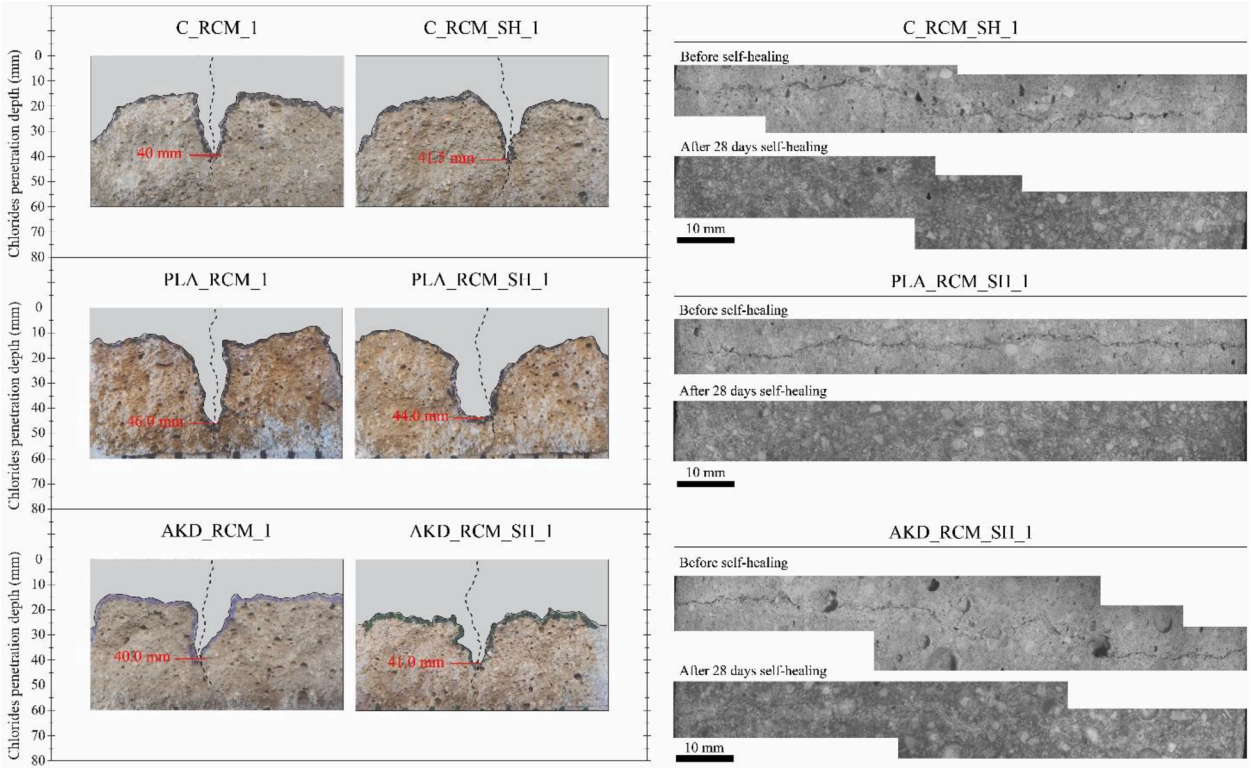

Fig. 8. Light microscope images of the specimens with and without self-healing tested through the RCM test. (left) chloride penetration (highlighted in grey) and maximum chloride penetration depth ("Mixture_RCM_1" with no prior self-healing, "Mixture_RCM_SH_1" with prior 28 days of self-healing). The dotted line shows the location of the crack; (right) surface crack images of the self-healed specimens before and after self-healing exposure (water submersion at laboratory conditions for 28 days).

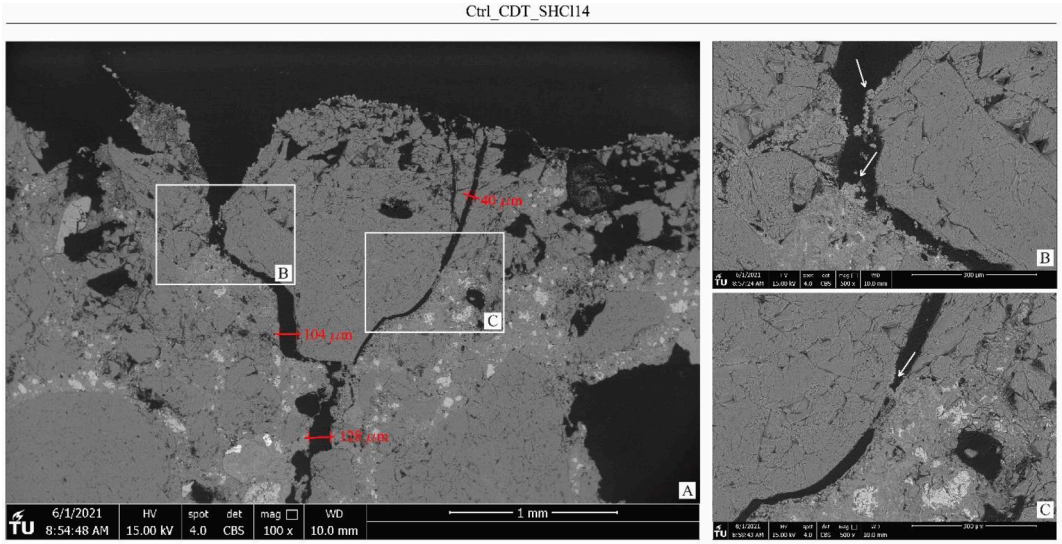

Fig. 9. SEM micrograph of the top (surface) part of specimen Ctrl_CDT_SHCl14. A) Overview of the top part of the specimen (magnification of 100x); B-C) Partial or complete (crack-bridging) self-healing of cracks due to precipitation of self-healing products, indicated by white arrows (magnification of 500x).

diffusion tests are better reproducing the real conditions to which structures are exposed, their results might differ significantly from those obtained through standard migration tests. For instance, the more impermeable the mixture is, the higher the scatter among different methods of calculations. In this study, the chloride diffusion coefficients measured according to the NT Build 443 were two to three times smaller than the migration coefficients measured through the NT Build 492, as visible in Fig. 16.

It is out of the scope of the present paper to clarify the reason why such a high difference was found between the results of the two methods, that depends on the both the material quality in addition to the calculation method [26]. Although different, the observed trend was the same for both methods, i.e. that the control (reference) specimens appeared to show the least resistance against chloride ingress, followed by specimens of the mix to which AKD based healing was added, while specimens made from PLA based healing agent amended mix showed the

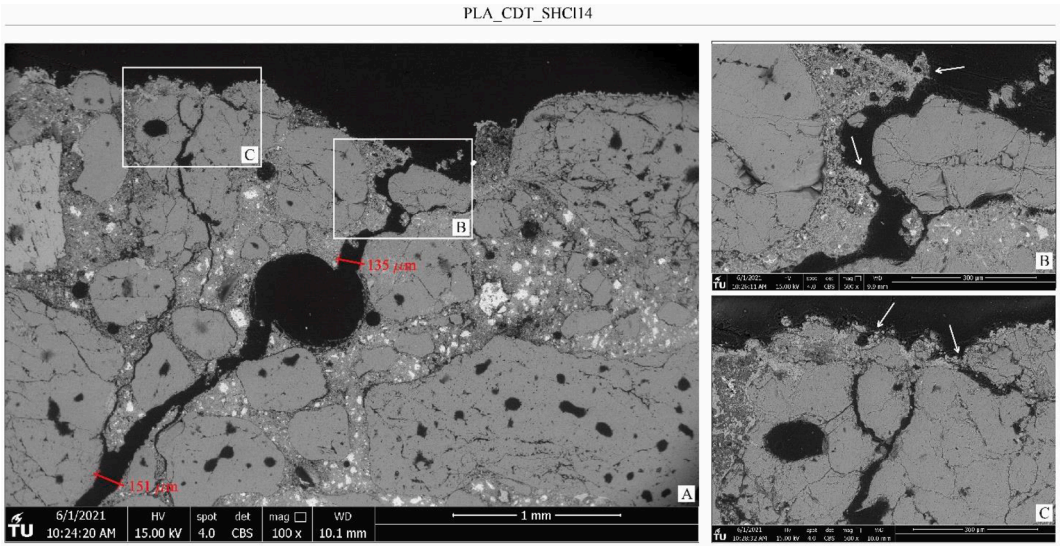

Fig. 10. SEM micrograph of the top part of specimen PLA_CDT_SHCl14. A) Overview of the top part of the specimen (magnification of 100x); B-C) Partial or complete (crack-bridging) self-healing of cracks due to precipitation of self-healing products, indicated by white arrows (magnification of 500x).

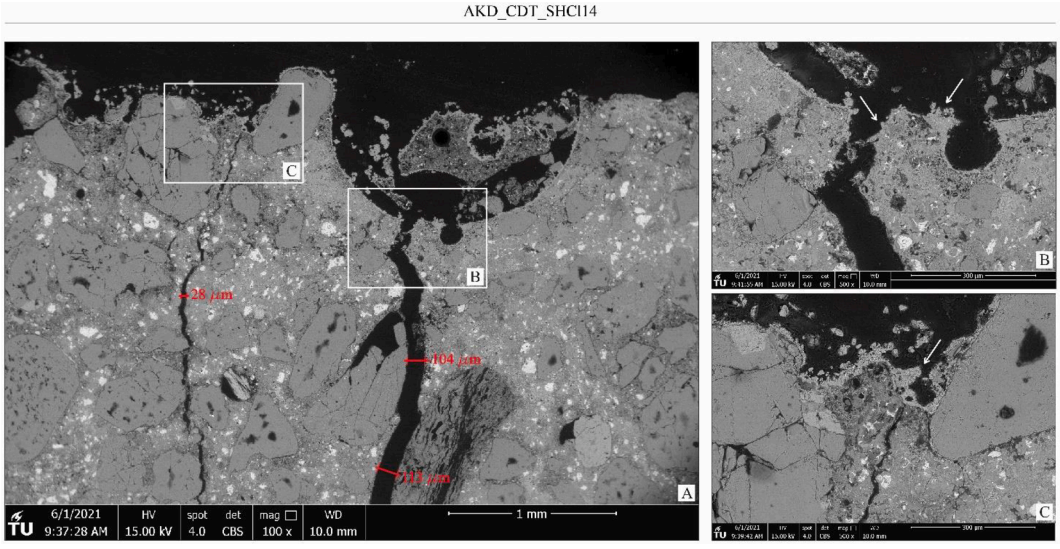

Fig. 11. SEM micrograph of the top part of specimen PLA_CDT_SHCl14. A) Overview of the top part of the specimen (magnification of 100x); B-C) Partial or complete (crack-bridging) self-healing of cracks due to precipitation of self-healing products, indicated by white arrows (magnification of 500x).

highest chloride ingress resistance. A relationship between the degree of resistance to chloride ingress and pore volume or pore size distribution of the mortar matrix might be expected.

According to the MIP results (Fig. 15), specimens derived from the PLA mixture showed the lowest pore volume, while AKD specimens showed the highest presence of pores ranging between 1 and 10 µm. Both these characteristics are representative for a densification of the matrix in comparison to specimens derived from the Ctrl mixture, therefore showing higher resistance to chloride penetration. The lower pore volume of PLA mix derived specimens might be due to the somewhat higher setting retardation as previously reported [21], that could result in a more homogeneous formation of hydration products leading to a denser mortar microstructure. Compared to Ctrl mixture specimen, those derived from the AKD mixture were found to feature higher presence of small size pores (0.01–0.1 µm), characteristics for a denser microstructure.

Furthermore, thin sections of the upper (surface) part of each specimen (Fig. 17) revealed the presence of a thin calcium carbonate layer formed at the surface of PLA and AKD based specimens. In combination with a denser microstructure, the presence of this layer might also have been responsible for the observed higher chloride penetration resistance of specimens derived from both the mixtures. Similar calcium carbonate layers at the surface of mortar specimens were also observed by De Muynck et al. [27], who investigated the degradation resistance of specimens from mortar mixtures subjected to different surface treatments. As a result, in that study it was demonstrated that bacterial carbonate precipitation improved the durability of cementitious materials. However, differently from their study, in the present study the bacterial healing agents were added to the mortar mix and not applied as a surface treatment. The presence of a calcium carbonate layer on top of both PLA and AKD specimens but not on the Ctrl specimens suggests that its formation and consequent higher chloride penetration resistance is related to the healing agent addition. More research to define the mechanism through which this occurs is needed.

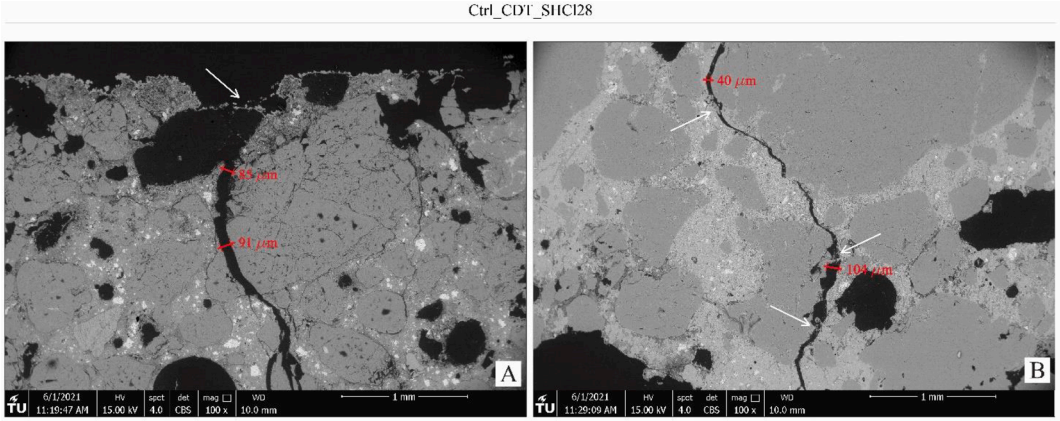

Fig. 12. SEM micrograph of specimen Ctrl_CDT_SHCl28. A) Top part of the cracked specimen showing partial or complete self-healing of cracks due to precipitation of self-healing products, as indicated by white arrows (magnification of 100x); B) Part of the specimen located at 40 mm down from the surface, indicating by white arrows partial or complete self-healing (magnification of 100x).

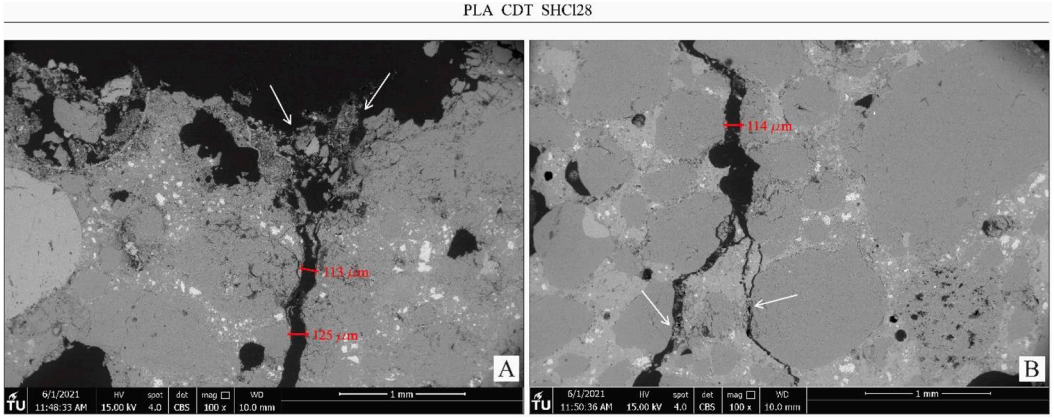

Fig. 13. SEM micrograph of specimen PLA_CDT_SHCl28. A) Top part of the cracked specimen showing partial or complete self-healing of cracks due to precipitation of self-healing products, as indicated by white arrows (magnification of 100x); B) Part of the specimen located at 40 mm down from the surface, indicating by white arrows partial or complete self-healing (magnification of 100x).

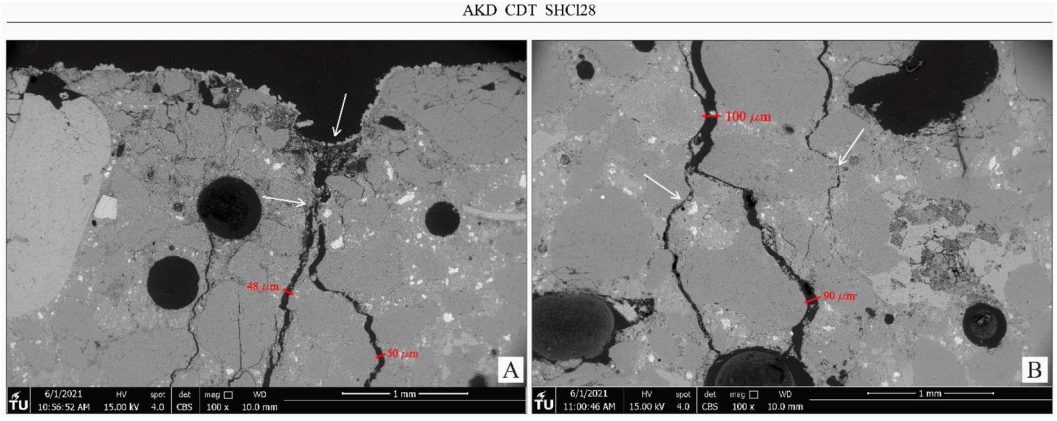

Fig. 14. SEM micrograph of specimen AKD_CDT_SHCl28. A) Top part of the cracked specimen showing partial or complete self-healing of cracks due to precipitation of self-healing products, as indicated by white arrows (magnification of 100x); B) Part of the specimen located at 40 mm down from the surface, indicating by white arrows partial or complete self-healing (magnification of 100x).

4.2. Influence of crack width on chloride penetration

The relation between the initial effective crack width, $w_{eff,i}$, and the effective crack mouth opening displacement, $CMOD_{eff}$, for each specimen as well as the relation between the effective crack width and the chloride penetration depth is shown in Fig. 18.

According to Fig. 18 (left), the relation between the $w_{eff,i}$ and $CMOD_{eff}$ is apparently linear but also that some variation occurs that is partly due to the fact that crack closure after relaxation overall varied among different specimens (see also Table 4-5). A maximum difference

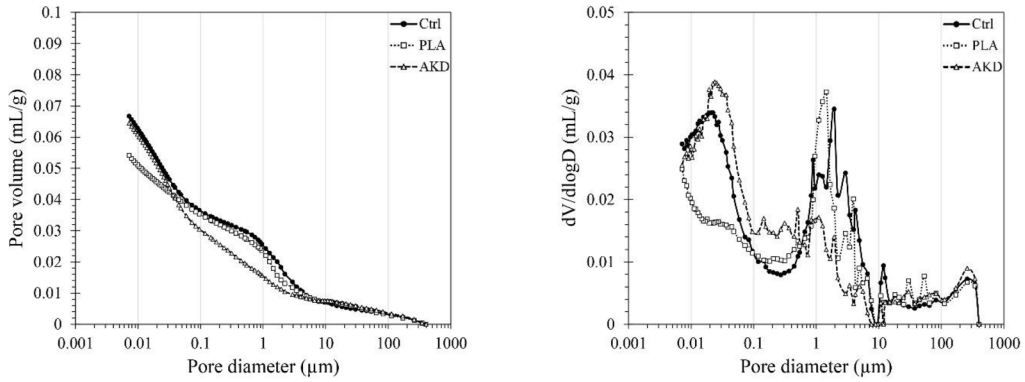

Fig. 15. (left) pore volume in relation to the pore size diameter distribution for the Ctrl, PLA and AKD specimens; (right) dV/dlogD in relation to the pore size diameter distribution for Ctrl, PLA and AKD specimens.

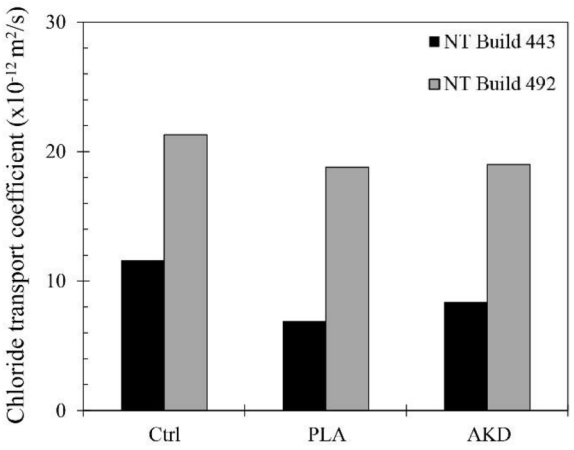

Fig. 16. Chloride diffusion and migration coefficients of sound specimens according to NT Build 443 and NT Build 492.

of 21 μm was observed between the determined CMOD and effective crack width for cracks ranging between 152 and 205 μm. However, according to SEM analysis on cross sections conducted in this study, the crack widths below the surface of the specimens were overall lower than those at the surface as determined by optical microscopy analysis as well as through the Instron analyses. Furthermore, SEM analysis revealed the presence of internal multiple (micro) cracks beside the main induced crack. These observations clarify the need for internal crack characterization, what is often omitted in studies as mostly only the crack width at the surface of specimens is considered. That the internal crack morphology shows very poor relationship with the crack width at the surface of specimens as shown in this study may lead expectedly to consequences for chloride ingress resistance and degree of self-healing of cracks. Fig. 18 (right) shows indeed a poor, if at all, relationship between observed chloride penetration depth and determined effective crack width.

Chloride penetration after RCM test of around 46 mm was measured for both PLA_RCM_1 and AKD_RCM_2-3, even though they had a crack width of 168 μm, 200 μm and 205 μm, respectively. For specimens with a crack width ranging between 170 μm and 185 μm chlorides penetrated from around 35 mm to a maximum of around 45 mm. Similar relationship is visible for the specimens subjected to the chloride diffusion test. For specimens submerged in NaCl solution for 14 days, the chloride penetration depths in AKD_CDT_Cl14 and PLA_CDT_Cl14 (both with a crack width of 172 μm) were equal to 34 mm and 35 mm, respectively, while that for the Ctrl_CTD_Cl14 was equal to 42 mm even though its crack width was equal to 162 μm. At the same time, lower chloride penetration depth difference was measured for the specimens submerged for 28 days in NaCl solution (between 44.5 mm and 47 mm), while the crack widths ranged between 155 μm and 178 μm. Looking at the influence that crack width has on chloride penetration according to the present study, the results suggest that the chloride transport coefficient is not clearly depending on the width of cracks ranging between 152 μm and 205 μm. The lack of negative influence that micro-cracks have on chloride transport was pointed out by other studies [12–14], but it was found that it was limited to crack widths ranging between 25 μm and 60 μm. Cracks considered in the present study were however substantially wider and the observed scatter in data suggest that for crack width ranging from 152 to 205 μm the chloride transport is largely independent from the width of the cracks themselves. These results agree with what was pointed out by Djerbi et al. [28], who suggested that the chloride transport coefficient increases for crack widths up to 80 μm. On the other hand, the chloride transport coefficient gets constant (i.e. equal to the chloride transport coefficient in free solution) for cracks wider than 80 μm.

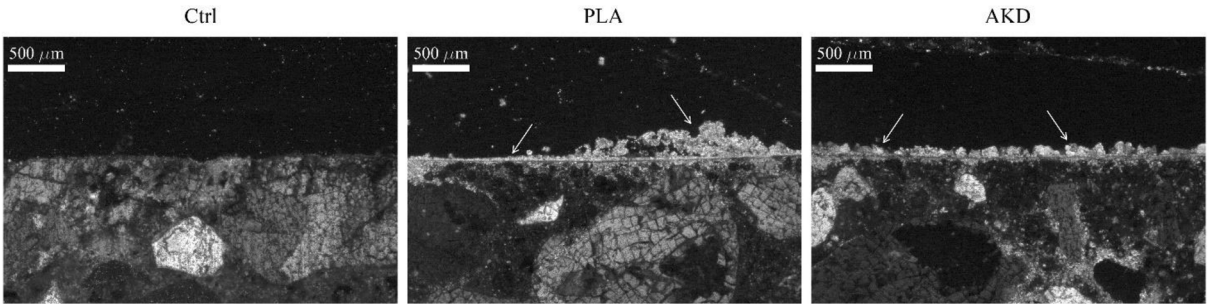

Fig. 17. Thin section micrographs of the upper (surface) part of one specimen from Ctrl (left), PLA (centre) and AKD (right) mixtures at 56 days of age. White arrows indicate calcium carbonate precipitates at the surface of specimens.

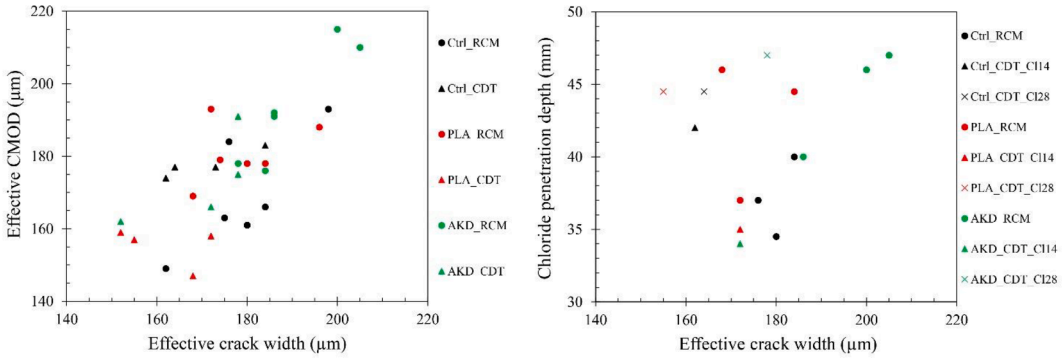

Fig. 18. (left) Relation between the effective crack mouth opening displacement (CMOD) according to the cracking procedure described in Section 2.3.3 and the final effective crack width measured through microscopy analysis; (right) Relation between chloride penetration depth in non-self-healed specimens and the final effective crack width measured through microscopy analysis.

4.3. Influence of self-healing on chloride penetration

The crack width of specimens tested through RCM ranged between 162 μm and 205 μm, while for specimens subjected to the chloride diffusion test it ranged between 152 μm and 184 μm. Microscopy analysis revealed that cracks in all specimens, irrespective of the mix they were derived from, completely healed at the crack surface after 28 days of water submersion (i.e. SHC = 100%). However, the beneficial effect that self-healing might have on chloride penetration can be evaluated only by looking at the specimens subjected to chloride diffusion test (Fig. 19).

Fig. 19 (left) shows that the average chloride penetration depth of the specimens tested through RCM before self-healing was equal to 37.2 mm, 42.5 mm and 44.3 mm for specimens of Ctrl, PLA and AKD mixtures, respectively. Even though previous studies reported that the migration coefficient of concrete is about twice the value of its immersion diffusion coefficient [29–30], the chloride penetration depth for the specimens tested in this study is overall similar among the different methodologies. Differently from previous studies, the specimens herewith investigated were cracked beforehand. The presence of cracks (with no self-healing) is likely the leading factor influencing the depth at which chlorides could penetrate regardless the application of the migration or the diffusion test procedure. Complete crack closure occurred for all the specimens after 28 days of water submersion. However, the average chloride penetration depth of self-healed specimens after RCM was equal to 38.2 mm, 41.0 mm and 43.8 mm for specimens of Ctrl, PLA and AKD mixtures, respectively, thus not markedly different from those before self-healing. The results of the RCM test therefore do not show a positive effect of self-healing on chloride penetration resistance. This fact is likely related to the degree of self-healing occurring in the specimens as well as to the applied methodology. According to the conducted SEM analysis, self-healing of cracks was only established by a thin layer of precipitates at the crack mouth as well as locally through crack-bridging due to the formation of precipitates at specific but limited number of locations along the crack depth. Higher degree of self-healing at the crack mouth and consequent lower precipitation in the crack depth is likely due to the higher availability of CO_2 and O_2 at the specimen surface, as already reported by others [3]. The lack of an in-depth dense and compact layer of precipitates would leave a preferential path for chlorides to penetrate the specimens when migrating thanks to the application of the voltage difference implied by the RCM test. Similarly, Yoon and Schlangen [12] reported that the beneficial effects of self-healing could be observed only in their long-term free chloride diffusion experiment (i.e. keeping the cracked specimens submerged in NaCl solution for, in their case, 472 days), and not in their short term RCM test. Since the cracks induced in the present study were also 5–6 times larger than those that they induced, complete in-depth crack healing was even more difficult to obtain. Crack-healing through bridging of the crack at various locations along the crack depth is thus apparently insufficient to significantly delay ingress of chlorides when subjected to a potential difference as applied in the RCM test. On the other hand, the free chloride diffusion test results demonstrated the degree at which chloride penetration decreases thanks to self-healing. The beneficial influence of the formation of self-healing products at the crack mouth was more accentuated for specimens exposed to 14 days of NaCl solution. After 14 days of submersion in NaCl solution, the decrease of chloride penetration depth thanks to self-healing was equal to 18 mm, 15.5 mm and 12 mm for specimens of Ctrl, PLA and AKD mixtures, respectively. However, this difference decreased in time as after 28 days of submersion in NaCl solution, the depth decrease was limited to 3 mm, 6.5 mm and 11 mm for the respective specimens. In agreement with what has been already reported by others [12], the chloride penetration depth increased for longer exposure to NaCl solution, regardless the occurrence of self-healing. The beneficial effect of self-healing on chloride penetration was more accentuated for shorter exposure, suggesting that the occurrence of a thin self-healing product

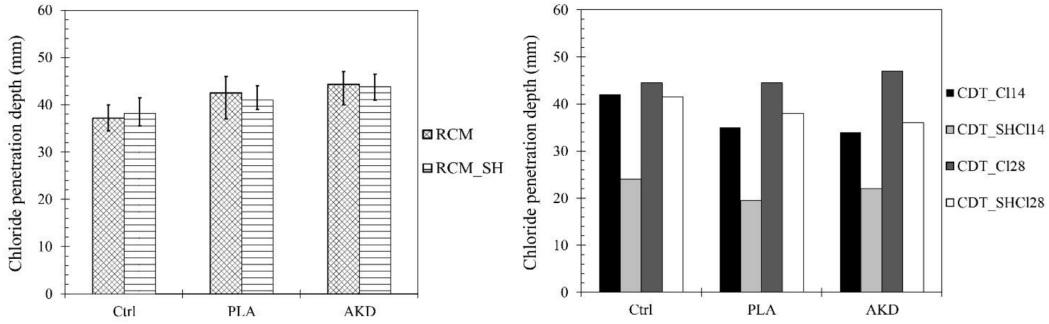

Fig. 19. (left) Chloride penetration depth in specimens derived from each mixture as determined by RCM Test before and after self-healing; (right) Chloride penetration depth measured for specimens subjected to the Chloride Diffusion Test before and after self-healing.

layer would initially block the chlorides from penetrating in the crack depth. However, even though the penetration depth in self-healed specimens after 28 days of submersion in NaCl solution was still lower than that of un-healed specimens, self-healing could not block chlorides from penetrating the material. Since the crack does not get completely filled with self-healing products over its entire depth, the empty portions of the crack, presumably filled with pore solution, allows relatively fast diffusion of chloride ions. Hence, for cracks of around 150–200 μm as reported in this study, self-healing is beneficial since it retards the penetration of chlorides, however not to the extent of sound specimens. The degree to which this behaviour could be functionally and economically beneficial needs to be assessed with further research. It is worth mentioning that this study investigated the performance of mortar specimens against chloride penetration, which does not have any coarse aggregate and related interfacial zone (ITZ), which highly (negatively) influences the transport properties of concrete. Furthermore, the high chlorides concentration of both tests' solutions as well as the application of an external electric field for the RCM test hardly represent the real conditions to which structures are generally exposed to in practice. As a consequence, the results of this study should be only considered as a potentially representative indicator of possible practical applications of concrete structures. For instance, structures are not continuously exposed to high levels of chloride such as infrastructures only occasionally exposed to de-icing salts or concrete located in or above the splash zone of marine waters may benefit from delayed chloride ingress due to self-healing of cracks.

Overall, all specimens derived from mortar mixtures investigated in this study showed an increase in penetration resistance thanks to self-healing (see Fig. 19) as also the autogenous self-healing capacity of the control specimens showed 100% self-healing. An improved chloride ingress resistance of specimens derived from mixes to which either the PLA- or AKD-based healing agent were added could therefore not be observed since the cracks induced in the present study were in the range of those that can be theoretically autogenously self-healed by mortar (i.e. around 150 μm [3]). Subsequent studies on specimens featuring larger cracks, e.g. in the range from 200 to 400 μm and typically above the autogenous self-healing capacity of mortar, are required to clarify whether addition of PLA- or AKD-based healing agents (or any other) significantly reduce chloride resistance of derived specimens in comparison to control mix designs.

5. Conclusions

The aim of this study was to assess the chloride transport properties of PLA- and AKD-based healing agent amended mixtures as well as to investigate the possible beneficial influence that stimulated self-healing might have on chloride penetration resistance in comparison to that of traditional Portland cement mortar. From the experimental campaign reported in the present study, the following major conclusions can be drawn:

- The chloride penetration resistance of intact (non-cracked) specimens derived from self-healing mixtures was higher than of those derived from Portland cement based mixture. Lower chloride migration and diffusion coefficients were found to be related to the lower pore volume for the PLA-based specimens and a higher quantity of smaller pores for AKD-based specimens mixture according to MIP tests. Furthermore, a layer of calcium carbonate precipitates was observed to be formed at the surface of both PLA and AKD specimens, what was thought to contribute further to the resistance to chlorides penetration.
- Chloride penetration through cracks in the range from 150 to 200 μm width appears not dependent on the crack width anymore as penetration rate appears already maximal in all.
- Microscopy analysis demonstrated that all the specimens could completely self-heal the cracks at the surface of the specimens after 28 days of water submersion. The maximum width that specimens could heal was 198 μm for Ctrl, 196 μm for PLA and 205 μm for AKD specimens.
- SEM analysis demonstrated the presence of a layer of self-healing products at the crack mouth. This layer appeared thicker in PLA and AKD based specimens than in control specimens. Deeper in the crack, self-healing was more limited and mainly present at certain locations only, leaving the crack depth largely un-healed.
- The possible beneficial influence of self-healing on chloride penetration of cracked specimens could not be observed in specimens subjected to the RCM test.
- Cracked and self-healed specimens subjected to the free chloride diffusion test showed a positive effect on resistance towards chloride penetration. The results of this study suggest that the self-healing products layer forming at the crack mouth can initially mitigate chloride penetration through the crack due to blocking of chlorides at the specimen surface. However, since no complete self-healing occurred over the entire crack depth, it appears likely that the empty part of the cracks, supposedly filled with pore solution, afford chloride migration over time, hence offering a preferential path for chlorides to penetrate. The impact of crack-healing on improvement of chloride penetration resistance for practical applications needs to be further assessed but may be relevant for concrete structures subjected to only temporal exposure to chlorides such as infrastructures occasionally exposed to de-icing salts or concrete located in or above the splash zone of marine waters.

CRediT authorship contribution statement

Emanuele Rossi: Conceptualization, Methodology, Investigation, Writing – original draft. **Rahul Roy:** Investigation, Writing – review & editing. **Oguzhan Copuroglu:** Writing – review & editing, Supervision. **Henk M. Jonkers:** Writing – review & editing, Supervision, Project administration.

Declaration of Competing Interest

The authors declare that they have no known competing financial interests or personal relationships that could have appeared to influence the work reported in this paper.

Acknowledgements

Financial support from Netherlands Organization for Scientific Research NWO-TTW (grant ALWGK.2016.021) for this work is gratefully acknowledged.

References

[1] M. De Rooij, K. Van Tittelboom, N. De Belie, E. Schlangen, Self-healing phenomena in cement-based materials: state-of-the-art-report of RILEM Technical Committee 221-SHCRILEM state of the art report, Springer, Vol, Dordrecht, Netherlands, 2013, p. 11.
[2] N. Hearn, Self-sealing, autogenous healing and continued hydration: what is the difference? Mater. Struct. 31 (8) (1998) 563–567, https://doi.org/10.1007/bf02481539.
[3] N. De Belie, E. Gruyaert, A. Al-Tabbaa, P. Antonaci, C. Baera, D. Bajāre, et al., A review on self-healing concrete for damage management of structures, Materials Interface Sci. 5 (17) (2018) 1800074, https://doi.org/10.1002/admi.201800074.
[4] S. Jacobsen, J. Marchand, H. Hornain, SEM observations of the microstructure of frost deteriorated and self-healed concretes, Cem. Concr. Res. 25 (8) (1995) 1781–1790.
[5] H.-W. Reinhardt, M. Jooss, Permeability and self-healing of cracked concrete as a function of temperature and crack width, Cem. Concr. Res. 33 (7) (2003) 981–985.
[6] M. Şahmaran, İ.Ö. Yaman, Influence of transverse crack width on reinforcement corrosion initiation and propagation in mortar beams, Can. J. Civ. Eng. 35 (3) (2008) 236–245.
[7] C. Edvardsen, Water permeability and autogenous healing of cracks in concrete, in: Innovation in concrete structures: Design and construction, Thomas Telford Publishing, 1999, pp. 473–487.

[8] C.-M. Aldea, W.-J. Song, J.S. Popovics, S.P. Shah, Extent of healing of cracked normal strength concrete, J. Mater. Civ. Eng. 12 (1) (2000) 92–96.
[9] C.A. Clear, *The effects of autogenous healing upon the leakage of water through cracks in concrete* (No, Tech Rpt. 559) (1985).
[10] A. Darquennes, K. Olivier, F. Benboudjema, R. Gagné, Self-healing at early-age, a way to improve the chloride resistance of blast-furnace slag cementitious materials, Constr. Build. Mater. 113 (2016) 1017–1028.
[11] M. Sahmaran, G. Yildirim, T.K. Erdem, Self-healing capability of cementitious composites incorporating different supplementary cementitious materials, Cem. Concr. Compos. 35 (1) (2013) 89–101.
[12] I.-S. Yoon, E. Schlangen, Experimental examination on chloride penetration through micro-crack in concrete, KSCE J. Civ. Eng. 18 (1) (2014) 188–198.
[13] M. Ismail, A. Toumi, R. François, R. Gagné, Effect of crack opening on the local diffusion of chloride in cracked mortar samples, Cem. Concr. Res. 38 (8-9) (2008) 1106–1111.
[14] M. Şahmaran, Effect of flexure induced transverse crack and self-healing on chloride diffusivity of reinforced mortar, J. Mater. Sci. 42 (22) (2007) 9131–9136.
[15] L. Ferrara, T. Van Mullem, M.C. Alonso, P. Antonaci, R.P. Borg, E. Cuenca, A. Jefferson, P.-L. Ng, A. Peled, M. Roig-Flores, M. Sanchez, C. Schroefl, P. Serna, D. Snoeck, J.M. Tulliani, N. De Belie, Experimental characterization of the self-healing capacity of cement based materials and its effects on the material performance: A state of the art report by COST Action SARCOS WG2, Constr. Build. Mater. 167 (2018) 115–142.
[16] Van Mullem, T., Caspeele, R., & De Belie, N. (2019). The influence of SAPs on chloride ingress in cracked concrete. In MATEC Web of Conferences (Vol. 289, p. 08007). EDP Sciences.
[17] X. Wang, F. Xing, M. Zhang, N. Han, Z. Qian, Experimental study on cementitious composites embedded with organic microcapsules, Materials 6 (9) (2013) 4064–4081.
[18] M. Maes, K. Van Tittelboom, N. De Belie, The efficiency of self-healing cementitious materials by means of encapsulated polyurethane in chloride containing environments, Constr. Build. Mater. 71 (2014) 528–537.
[19] B. Van Belleghem, P. Van den Heede, K. Van Tittelboom, N. De Belie, Quantification of the service life extension and environmental benefit of chloride exposed self-healing concrete, Materials 10 (1) (2017) 5.
[20] C.M. Vermeer, E. Rossi, J. Tamis, H.M. Jonkers, R. Kleerebezem, From waste to self-healing concrete: A proof-of-concept of a new application for polyhydroxyalkanoate, Resour. Conserv. Recycl. 164 (2021) 105206, https://doi.org/10.1016/j.resconrec.2020.105206.
[21] E. Rossi, C.M. Vermeer, R.M. Mors, R. Kleerebezem, O. Copuroglu, H.M. Jonkers, On the applicability of a precursor derived from organic waste streams for bacteria-based self-healing concrete. Frontiers, Built Environment 7 (2021).
[22] N.T. Build, 443,, Nord Test Method for accelerated chloride penetration in hardened concrete and other cement-based materials, Nordic Council of Ministers, ESPOO, Finland, 1995.
[23] RILEM TC 178-TMC (2002). Testing and Modelling Chloride Penetration in Concrete: Analysis of Total Chloride Content in Concrete. Materials and Structures, vol. 35, no. 253, 2002, pp. 583–585.
[24] N.T. Build, 492., Concrete, mortar and cement-based repair materials: Chloride migration coefficient from non-steady-state migration experiments, Nordic Council of Ministers, Finland, 1999.
[25] U.H. Jakobsen, D.R. Brown, Reproducibility of w/c ratio determination from fluorescent impregnated thin sections, Cem. Concr. Res. 36 (8) (2006) 1567–1573.
[26] C. Andrade, M. Castellote, C. Alonso, C. González, Non-steady-state chloride diffusion coefficients obtained from migration and natural diffusion tests. Part I: Comparison between several methods of calculation, Mater. Struct. 33 (1) (2000) 21–28.
[27] Willem De Muynck, Dieter Debrouwer, Nele De Belie, Willy Verstraete, Bacterial carbonate precipitation improves the durability of cementitious materials, Cem. Concr. Res. 38 (7) (2008) 1005–1014.
[28] A. Djerbi, S. Bonnet, A. Khelidj, V. Baroghel-bouny, Influence of traversing crack on chloride diffusion into concrete, Cem. Concr. Res. 38 (6) (2008) 877–883.
[29] K. Li, Durability design of concrete structures: Phenomena, modeling, and practice, John Wiley & Sons, 2017.
[30] F. Ren, L. Li, W. Wang, C. Zhou, Transport properties of surface layers from full-scale reinforced concrete member, Structural Concrete 22 (2021) E1062–E1073.